Improving Apparent Impedance Calculations in Systems With IBRs

Michael Rader
Minnesota Power

Ryan McDaniel, Josh LaBlanc, Kale McCarthy, and Bishal Lamichhane
Schweitzer Engineering Laboratories, Inc.

Presented at the
62nd Annual Midwest Power Systems Conference
Saint Paul, Minnesota
November 10–12, 2026

Originally presented at the
53rd Annual Western Protective Relay Conference, October 2026

Improving Apparent Impedance Calculations in Systems With IBRs

Michael Rader, *Minnesota Power*
Ryan McDaniel, Josh LaBlanc, Kale McCarthy, and Bishal Lamichhane, *Schweitzer Engineering Laboratories, Inc.*

***Abstract*—The increasing penetration of inverter-based resources (IBRs) has introduced new challenges for transmission line distance protection. During faults, IBRs can produce significant interharmonic frequency content that is not fully attenuated by conventional phasor-estimation techniques in digital relays, resulting in oscillatory apparent impedance measurements. These oscillations can cause both overreach and underreach of distance elements, often requiring user-implemented security and dependability timers to maintain reliable operation.**

This paper examines the impact of interharmonic content on apparent impedance calculations calculated from the output of finite input response (FIR) filters with and without a replica current filter. Using a replica current filter preserves voltage-current alignment across all frequency components that pass through FIR filtering, significantly improving the stability of apparent impedance measurements.

Analytical examples, an electromagnetic transient simulation, and a field event involving an external fault on a transmission system supplied by 600 MW of wind generation are presented. Results demonstrate that FIR methods without a replica current filter can produce substantial apparent impedance oscillations, including a documented Zone 1 distance element overreach for an external fault. Relays employing a replica current filter maintained a stable apparent impedance estimate and remained secure under the same conditions. The paper also shows how a replica current filter improves resilience to both dc offset and interharmonic frequency content while preserving fast relay operating times.

The results demonstrate that a replica current filter can significantly improve the security and dependability of distance protection in IBR-dominated power systems, reducing or eliminating the need for user-applied reliability timers and providing a practical path toward more robust apparent impedance measurement.

I. Introduction

Power system generation sources have historically required relatively simple models to explain their behavior during faults. In general, they provided a consistent nominal frequency (i.e., 60 Hz) regardless of system loading conditions or fault events. In addition to 60 Hz content, harmonics, which are integer multiples of the fundamental frequency, are also present in power systems. Harmonics can result from various forms of magnetic core saturation, including transformer inrush and overexcitation.

Early digital relays operated with sampling rates as low as four samples per cycle (240 Hz on a 60 Hz system) [1]. To prevent signal aliasing, these relays employed a low-pass filter that attenuated frequencies above half the sampling rate (i.e., 120 Hz). The filtered current and voltage signals were then processed through a finite impulse response (FIR) filter. The two most common FIR implementations are the cosine filter (FIR_{COS}) and the Discrete Fourier Transform filter (FIR_{DFT}), both of which effectively reject harmonic content. Early digital relays operated on a highly constrained frequency spectrum, while the power system generated relatively little frequency content outside the rejection capabilities of the relay filtering process. However, because of the inductive nature of most power-system components, faults often produce a decaying dc offset in the current waveform. This dc component requires special consideration and represents the primary non-fundamental frequency component that relay designers need to address.

The FIR_{COS} filter is inherently effective at rejecting dc offsets, while FIR_{DFT} implementations require an additional filtering stage to further attenuate the decaying dc component associated with fault currents that can lead to distance element overreach [2]. Both filtering approaches have been used successfully for decades in digital relays and have provided reliable performance in systems dominated by high-inertia generation sources that produce power through electromagnetic induction.

Determining the behavior of inverter-based resources (IBRs) during fault conditions requires a much more complex model than that of conventional generation sources. In general, IBRs possess low inertia, and their power production and fault response are governed by firmware-controlled power electronic converters that transform dc power into ac power. These power electronics can introduce a much broader frequency spectrum into the voltage and current signals observed by protective relays, including interharmonic components (e.g., 60–120 Hz) that are only minimally attenuated by modern phasor-based relay filters. Furthermore, digital relay sampling rates have steadily increased and may now exceed 32 samples per cycle (1,920 Hz) with low-pass filter cutoff frequencies approaching 960 Hz. In earlier relay designs, the low-pass filter performed much of the work required to isolate the 60 Hz fundamental component and naturally attenuated even relatively low-frequency interharmonics. In contrast, modern phasor-based relays provide significantly less attenuation of low-frequency interharmonic content through either the low-pass filter or the FIR filter.

Failure to reject or otherwise account for interharmonic content can result in oscillations in the measured apparent impedance, a challenge that has been documented in simulation studies [3]. However, another challenge that is closely related is the reduced inertia in IBR-dominated systems. Distance

elements that rely on memory polarization have a dynamic characteristic in the apparent impedance plane, and reduced inertia can lead to unexpected locations of the characteristic in the apparent impedance plane. The instability of the apparent impedance calculation coupled with the erratic movement of the dynamic characteristic leads to poor distance element performance.

To address the challenge of reduced inertia, distance elements that do not rely on memory voltage have been proposed for transmission lines located near IBR installations [4]. These elements are polarized using fault loop quantities—either fault loop voltage (mho elements) or fault loop current (reactance and resistance elements)—and therefore maintain a fixed characteristic in the apparent impedance plane. These relays are commonly referred to as self-polarized distance elements. By eliminating the use of an external polarizing quantity, the dynamic movement of the operating characteristic is replaced by a static characteristic. Consequently, the distance element operates directly on the measured apparent impedance. A drawback of this approach is that self-polarized distance elements are inherently nondirectional and therefore require supervision by a directional element capable of maintaining dependable directional performance in low-inertia systems, such as a zero-sequence directional element (32G) or a time-domain directional element (TD32).

While self-polarized distance elements eliminate characteristic movement within the apparent impedance plane, it is equally important that the relay's apparent impedance measurement remain stable and accurate during fault conditions regardless of the type of source. Given the broad spectrum of frequency content produced by IBRs, including components that are not effectively rejected by modern FIR filters, the calculated apparent impedance may oscillate significantly if the ripples in the voltage and current phasors do not mutually cancel. If this additional frequency content is not properly addressed by the use of a replica current filter, even self-polarized distance elements may exhibit poor performance.

Recent research [5] has also explored wide-spectrum apparent impedance measurement techniques that extend beyond conventional phasor-based approaches. Rather than estimating apparent impedance from filtered fundamental frequency voltage and current phasors, these methods estimate apparent resistance and inductance directly from instantaneous fault loop quantities, allowing a broader range of frequency content to contribute to the measurement. As a result, wide-spectrum methods can provide improved impedance estimation in weak systems containing significant interharmonic content and fault resistance. While this paper focuses on improving conventional apparent impedance calculations through the use of a replica current filter, the wide-spectrum technique represents a complementary approach for future transmission line protection algorithms.

This paper shows that a significant contributor to apparent impedance oscillation is not merely the presence of interharmonic content, but rather the loss of alignment between the voltage and current nonfundamental frequency components that remain after relay filtering. Conventional phasor-processing techniques preserve voltage-current alignment only at the nominal system frequency, allowing residual interharmonic content to produce oscillatory phasor measurements. By implementing a replica current filter prior to phasor extraction, alignment is preserved across all frequency components that pass through relay FIR filtering, resulting in substantially improved apparent impedance stability. This paper demonstrates the effect through analytical examples, an electromagnetic transient simulation, and validation using a real-world transmission line misoperation involving 600 MW of inverter-based generation.

II. Apparent Impedance Measurements

Apparent impedance to the fault (Z_{APP}) is a complex number equal to the measured fault loop voltage divided by the measured fault loop current. In distance protection, there are six fault loops utilized (AB, BC, CA, AG, BG, CG). If a Phase A to Phase B fault occurs on a system, the apparent impedance ($Z_{APP[AB]}$) is simply a complex number equal to V_{AB}/I_{AB}. A proper apparent impedance calculation for a metallic fault will result in the fault loop impedance between the relay location and the fault location. This result should be fully independent of the generation source behavior [4].

Although apparent impedance forms the foundation of distance protection, modern distance relays generally do not operate directly on apparent impedance in North America. Most modern distance elements are polarized using quantities other than the fault loop voltage and current, causing the operating characteristic to become dynamic rather than solely dependent on the measured apparent impedance. Consequently, relay operation becomes a function of additional factors such as pre-fault loading, source impedance, source inertia, and fault direction.

The general equation for a mho distance element is given in (1). For the purposes of this discussion, two polarization methods are considered. The first uses positive-sequence memory voltage ($V1_{MEM}$), while the second uses $I \bullet Z_{R(OFFSET)} + V$.

$$\begin{aligned} &RE\left[S_{OP} \bullet S_{POL}^{\ *}\right] > 0 \\ &where \\ &S_{OP} = I \bullet Z_R - V \\ &S_{POL} = V_{POL} \end{aligned} \tag{1}$$

TABLE I
VOLTAGE POLARIZATION AND EFFECTS ON OFFSET

V_{POL}	Offset
$V1_{MEM}$	$-\left(\frac{V1_{MEM} - V}{I}\right)$
$I \bullet Z_{R(OFFSET)} + V$	$-Z_{R(OFFSET)}$

Using $V1_{MEM}$ produces a dynamic mho characteristic in which the offset is not settable [6]. As system conditions change, the size and location of the operating circle also changes. In contrast, using $I \bullet Z_{R(OFFSET)} + V$ produces a static mho characteristic in which the offset is user-defined and fixed.

As a result, the size and location of the operating characteristic remain constant in the apparent impedance plane.

Consider the radial system shown in Fig. 1. Under normal operating conditions the source impedance is equal to Z_{S1}. Under the contingency condition, the source impedance increases to $2{\cdot}Z_{S1}$. Two relays are installed at the relay location. Relay 1 uses $V1_{MEM}$ polarization, while Relay 2 uses $I \bullet Z_{R(OFFSET)} + V$ polarization. Both relays are configured with identical forward reach settings. For Relay 2, $Z_{R(OFFSET)}$ is set equal to Z_{S1}.

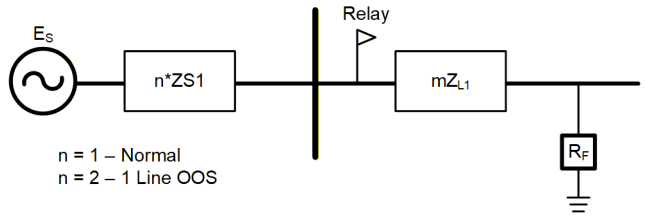


Fig. 1. Radial system with a fault located at mZ_{L1}.

Assume a fault occurs at location mZ_{L1} with fault resistance R_F for both system conditions. The resulting characteristics are shown in Fig. 2. Regardless of system condition, Relay 2 does not operate because the apparent impedance remains outside the static operating characteristic. Relay 1, however, restrains when n = 1 and operates when n = 2 even though the measured apparent impedance is unchanged. The weaker source causes the dynamic offset to move farther from the origin, increasing the operating circle sufficiently to encompass Z_{APP}. This example demonstrates that Relay 1 does not operate solely as a function of apparent impedance, whereas Relay 2 does.

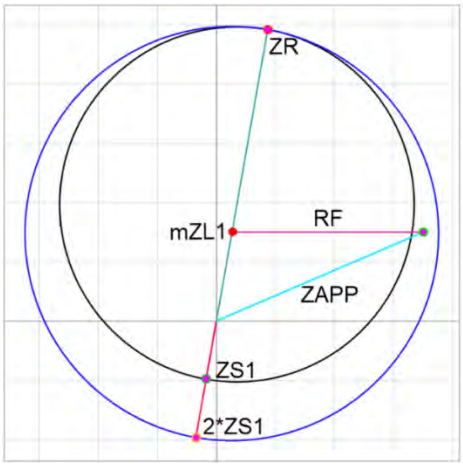


Fig. 2. Characteristics for Relay 1: black $n = 1$ and blue $n = 2$; characteristic for Relay 2: black only.

Two special cases of the static characteristic merit additional discussion: $Z_{R(OFFSET)} = 0$ and $Z_{R(OFFSET)} = Z_R$. The resulting characteristics are shown in Fig. 3. While either characteristic can be implemented using (1) with the appropriate polarization method, they can also be implemented through direct geometric evaluation of the apparent impedance. The characteristic represented by the blue circle is described by (2), whereas the black circle is described by (3). Equation (2) is derived from geometric evaluation of apparent impedance, while (3) is obtained from the traditional mho torque equation presented in the appendix.

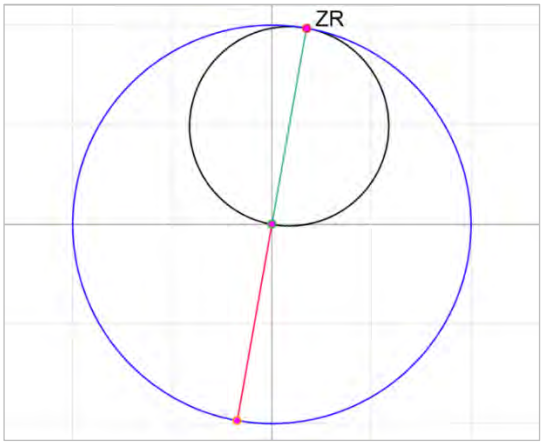


Fig. 3. $Z_{R(OFFSET)} = Z_R$ (blue) described by (2), $Z_{R(OFFSET)} = 0$ (black) described by (3).

$$\frac{|V|}{|I|} \angle |Z_R| \tag{2}$$

$$0 < \frac{|V^2|}{RE[V^* \bullet IZ]} \angle |Z_R| \tag{3}$$

where

$$IZ = I \bullet 1\angle Z_R$$

An important distinction between the two approaches is that (2) does not require phase-angle information from the measured voltages, currents, or reach settings. Equation (3), however, requires both magnitude and phase information, and the reach setting must be represented as a complex quantity where $\angle Z_R$ corresponds to the maximum torque angle. The term IZ in the denominator of (3) is referred to as replica current and is the measured current with the phase angle adjusted by the maximum torque angle.

For simplicity, the remainder of this paper focuses mainly on the performance of (2). Other distance element characteristics, such as quadrilateral characteristics that rely on linear boundaries rather than circles in the apparent impedance plane, are not considered. However, all distance characteristics benefit from improved apparent impedance calculations.

Distance relays that operate directly on the magnitude of apparent impedance were first applied for transmission line protection in the early twentieth century using balance beam relay technology [7]. Mathematically, this relay can be represented as a magnitude comparator by rearranging (2) into the form shown in (4), where the voltage magnitude is compared against the product of the current magnitude and a reach setting.

$$|I| \bullet |Z_R| > |V| \tag{4}$$

For faults within the set reach of the relay, (4) is true and the relay operates. For fault outside the relay reach, (4) is not true and the relay restrains. Because the magnitude operation removes phase-angle information from the measured signals, the relay is inherently nondirectional and therefore requires supervision by a separate directional element.

Although (4) represents one of the simplest implementations of a distance relay, relay behavior becomes significantly more complex when frequency components other than the nominal system frequency are present in the measured signals.

III. Voltage and Current Phasor Extraction

In this section, two phenomena that complicate accurate phasor estimation are examined: dc offset and interharmonic frequency content. To illustrate the impact of dc offset, consider the system shown in Fig. 4 where an impedance relay protects a transmission line with an impedance ZL. For simplicity, ZS and ZL are both assumed to be 1∠80°, and the source voltage magnitude is 100 V at 60 Hz.

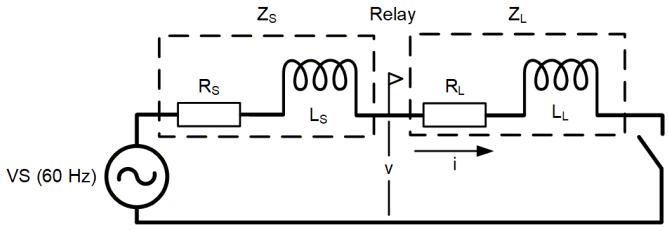


Fig. 4. Simple system with a 60 Hz source.

The impedance relay described by (4) requires accurate voltage and current magnitude measurements to operate correctly. If the relay reach magnitude is set equal to the line impedance magnitude and only the fundamental frequency components of voltage and current are extracted, the operating and restraining quantities remain balanced and the relay does not operate when the switch is closed. We can extend this reasoning and say that if the Z_{APP} is known, then (5) is true. In our example, $|Z_{APP}| = 1$ ohm.

$$|I_{60HZ}| \bullet |Z_{APP}| = |V_{60HZ}| \tag{5}$$

However, relay filtering is not a perfect bandpass filter that can extract only the 60 Hz component. Equation (6) represents the same equation but recognizing that the relay FIR filtering may not extract only the 60 Hz signal. In the following sections, we will answer whether or not (6) is true for all filtering methods.

$$|I_{FIR}| \bullet |Z_{APP}| = |V_{FIR}| \tag{6}$$

A. DC Offset Removal From Current

DC offset is a major source of transient measurement error, particularly in current signals immediately following fault inception. If the dc component is not adequately rejected, the apparent impedance may be underestimated, resulting in transient overreach. Fig. 5 compares several filtering approaches under a condition of significant dc offset.

Referring to Fig. 5, if the current magnitude (red trace) goes above the voltage magnitude (green trace), the relay underestimates the apparent impedance. FIR_{COS} exhibits only minor transient overreach. In contrast, FIR_{DFT} without any additional filtering produces unacceptable transient performance and is included primarily to demonstrate the necessity of dc offset removal. When a dc removal filter (DCR) is applied, FIR_{DFT} performance becomes comparable to FIR_{COS}, with a small speed advantage resulting from simultaneous calculation of the real and imaginary phasor components. $FIR_{DFT(REPLICA)}$ eliminates transient overreach entirely.

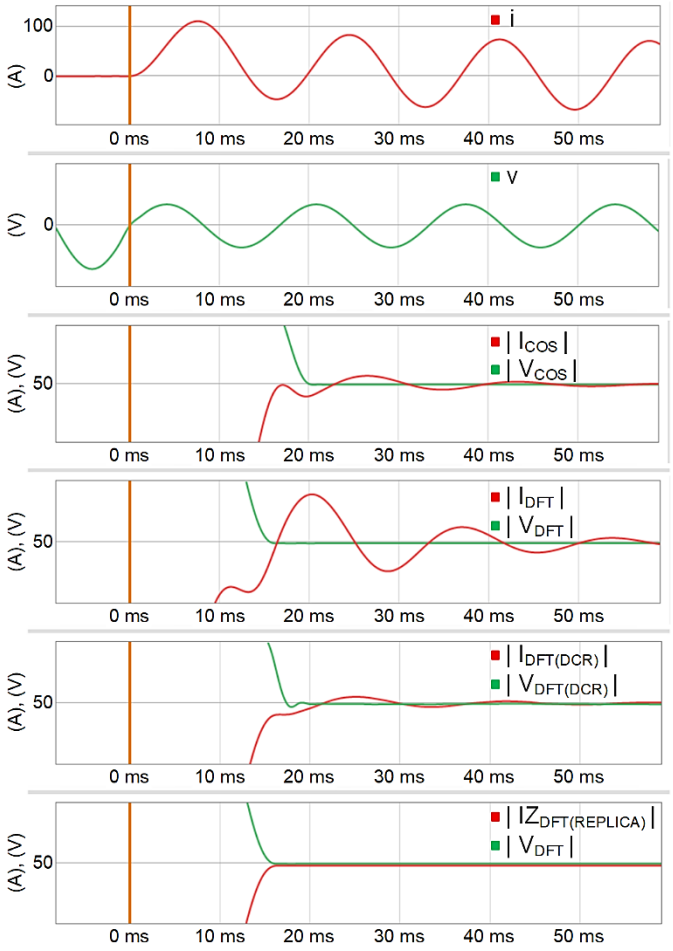


Fig. 5. Digital filter outputs when applying signals *v* and *i*.

The calculation of apparent impedance magnitude is shown in Fig. 6. Both FIR_{COS} and FIR_{DFT} temporarily underestimate the true apparent impedance during the transient period. In contrast, the $FIR_{DFT(REPLICA)}$ maintains an apparent impedance estimate that remains aligned with the expected value while maintaining exceptional speed. We can see that (6) only holds true if a replica current filter is used.

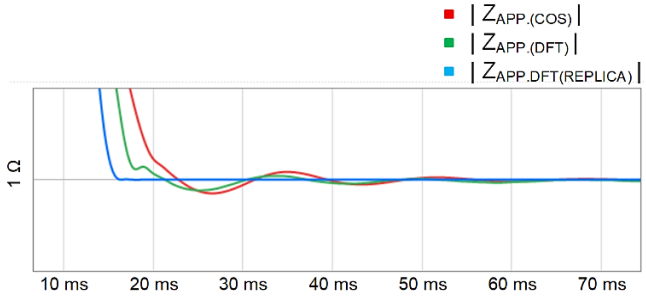


Fig. 6. Apparent impedance calculations of filtering techniques with dc content in the signal.

Fig. 7 shows a block diagram to explain how each filtered voltage and current signal is extracted in Fig. 5, and a brief description of each is given below.

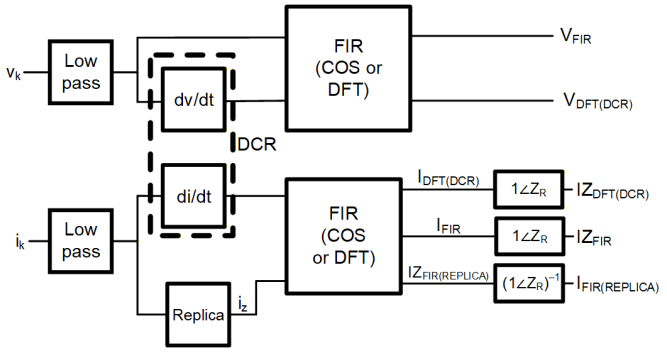


Fig. 7. Simplified filtering diagram.

The low-pass filter is primarily used to prevent signal aliasing. As relay sampling rates increase, the low-pass cutoff frequency also increases, placing greater reliance on downstream signal processing algorithms to isolate the desired fundamental frequency phasor.

A DCR, designated as di/dt for the current signal and dv/dt for the voltage signal, is a simple method to remove dc offset from the current signal while maintaining the phase-angle relationship between V and I. The DCR filter is only used with FIR_{DFT}. The di/dt filter takes the derivative of the input current, which removes standing dc content and reduces decaying dc content. However, taking the derivative of the current creates a 90 degree phase shift in the frequency domain and introduces a small group delay in the filter output. A method to remove this discrepancy between the voltage and current is to also take the derivative of the voltage signal as well. The addition of the DCR filter makes FIR_{DFT} and FIR_{COS} nearly equivalent in terms of dc removal.

The replica current filter calculates a current-derived quantity that reproduces the voltage expected across the protected line impedance (i_Z). When the line parameters are modeled accurately, the resulting signal removes dc offset while time aligning the current with the measured voltage. The replica current calculation therefore improves both transient accuracy and apparent impedance stability.

To explain replica current, we first start by calculating the voltage across the Z_L impedance in Fig. 4, represented by (7).

$$v = R_L \bullet i + L_L \frac{di}{dt} \tag{7}$$

If R_L and L_L match the values that make up the impedance Z_L, then v will be exactly equal to the voltage measured by the relay. However, (7) only has the proper voltage amplitude value for a fault that occurs at a single fault location. So, we scale (7) so that the amplitude value of the current is retained while keeping the dc offset removal and signal shifting, as shown in (8). In this example, (7) and (8) are identical, but (8) is generalized to allow use in conjunction with a distance element.

$$\begin{aligned} i_z &= \frac{R_R}{|Z_R|} \bullet i + \frac{L_R}{|Z_R|} \frac{di}{dt} \\ &where: \\ R_R &= |Z_R| \bullet \cos(\angle Z_R) \\ L_R &= \frac{|Z_R| \bullet \sin(\angle Z_R)}{2 \bullet \pi \bullet f_{nom}} \end{aligned} \tag{8}$$

Fig. 8 shows that the replica current (i_Z) is exactly equal to v before FIR filtering when the switch in Fig. 4 is closed.

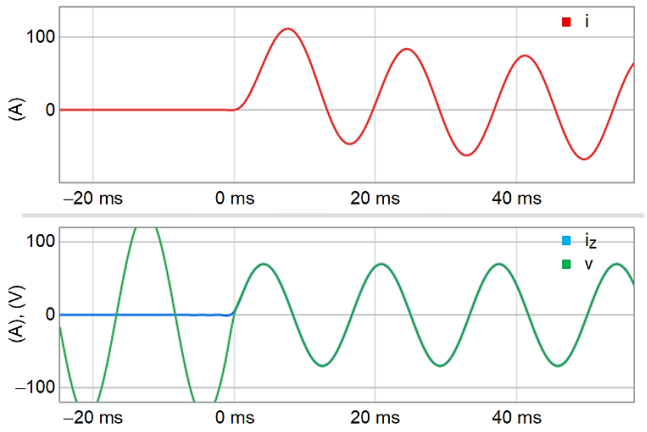


Fig. 8. i_Z relationship with v.

For the apparent impedance to be accurate when a replica current filter is used, it is important for the relay measured voltage to remain unaltered. It should not be subject to additional filtering because this corrupts the relationship with the replica current filter output. Therefore, the group delay that is introduced by the replica current filter should be accounted for without shifting or altering the voltage signal. Further, the potential transformer used should ideally maintain a good frequency response so that the additional frequency content impressed on the voltages aligns with the frequency content derived from the currents.

Fig. 7 also includes phase-angle adjustment multipliers to calculate replica current in the frequency domain ($IZ_{DFT[DCR]}$ and IZ_{FIR}) from the outputs of the FIR filter. These methods do not calculate replica current with a replica current filter. They simply phase adjust the nominal frequency content of the current only.

It is important to keep in mind that there are two versions of replica current depicted in Fig. 7: IZ that uses a replica current filter ($IZ_{FIR[REPLICA]}$) and IZ that does not use a replica current filter (IZ_{FIR}).

The multiplier to calculate $I_{FIR(REPLICA)}$ is shown to remove the phase shift introduced by the replica current filter. This calculation is not used in this paper but is included to complete the figure.

To complete the comparison between using a replica current filter and not, we calculate the time-domain representation of the filtered quantities v_{COS}, $iz_{COS(REPLICA)}$, and iz_{COS} using (9). We chose to only compare FIR_{COS} to $FIR_{COS(REPLICA)}$ because the DCR filter makes FIR_{DFT} perform similarly to FIR_{COS} in regard to dc offset removal.

$$\begin{aligned} i_{FIR}(t) &= \sqrt{2} \bullet mag(I_{FIR}) \bullet \cos\left[\omega \bullet t + ang(I_{FIR})\right] \\ v_{FIR}(t) &= \sqrt{2} \bullet mag(V_{FIR}) \bullet \cos\left[\omega \bullet t + ang(V_{FIR})\right] \end{aligned} \tag{9}$$

Next, we make a slight edit to (1) to define SOP when the relay reach (Z_R) is replaced with a known $|Z_{APP}|$, as shown in (10). $S_{OP(ZAPP)}$ is ideally zero and any non-zero value indicates signal content that is not adequately suppressed or processed by the FIR filter.

$$s_{OP(ZAPP)} = iz_{FIR} \bullet |Z_{APP}| - v_{FIR} \quad (10)$$

Because this is a transient simulation, we wait until the cosine filter window time (20 ms) after the switch closure to compare iz_{COS} and $iz_{COS(REPLICA)}$ to v_{COS}, as shown in Fig. 9.

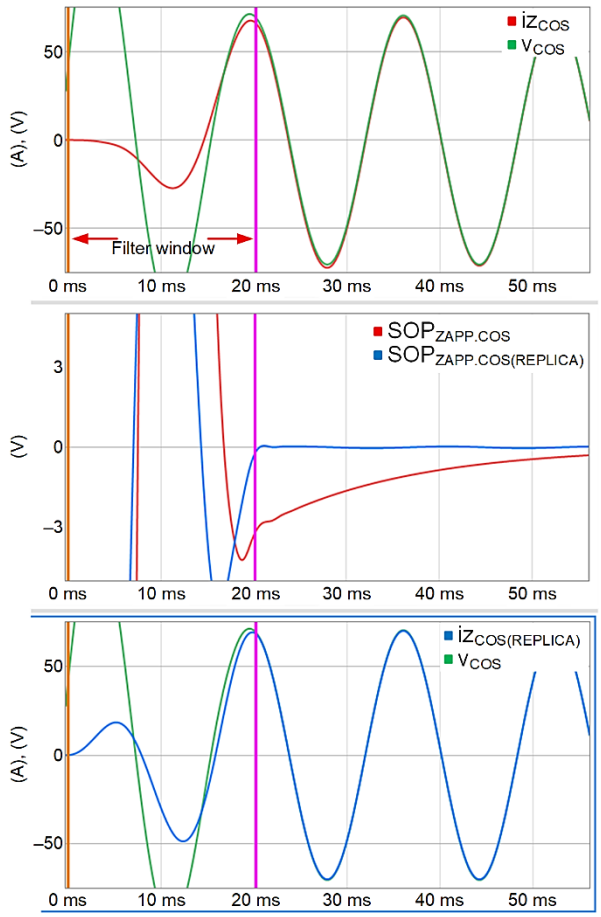


Fig. 9. Comparison of using a replica current filter versus not using a replica current filter.

We can see that using $iz_{COS(REPLICA)}$ is perfectly matched to v_{COS} once the filter window time has passed. However, there is a small difference between v_{COS} and iz_{COS} that remains as the cosine filter alone does not completely attenuate the dc offset in the current signal. This decaying dc difference is quite small, but it helps illustrate the slight mismatch between v_{COS} and iz_{COS}, which leads to a temporary apparent impedance underestimate.

B. Additional Off-Nominal Frequency Content

Although the preceding discussion focuses on dc offset, interharmonic frequency content presents a relatively newfound challenge. FIR filters effectively reject harmonics but provide limited attenuation of interharmonic frequencies. As shown by the frequency response of Fig. 10, frequency components between 60 Hz and 120 Hz may pass through the filters with little attenuation.

To demonstrate this behavior, the system in Fig. 4 is modified to include a 90-Hz component and the switch is simply a short circuit, as shown in Fig. 11. The resulting filter outputs in Fig. 12 show that none of the conventional FIR approaches completely reject the interharmonic signal. The residual interharmonic content appears as oscillatory ripple in the extracted voltage and current magnitudes.

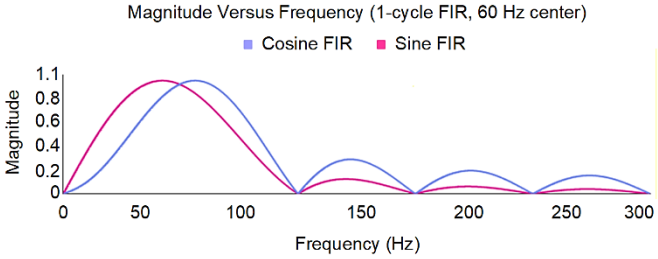


Fig. 10. FIR filter signal attenuation to interharmonic frequencies.

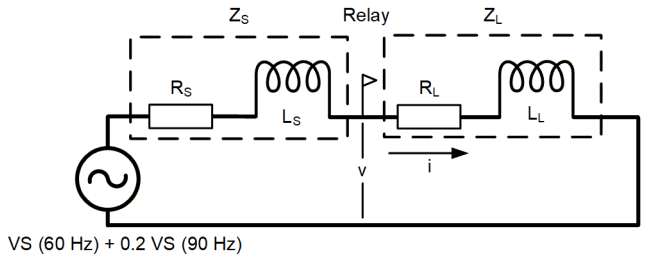


Fig. 11. Circuit with a 60 Hz and 90 Hz voltage source.

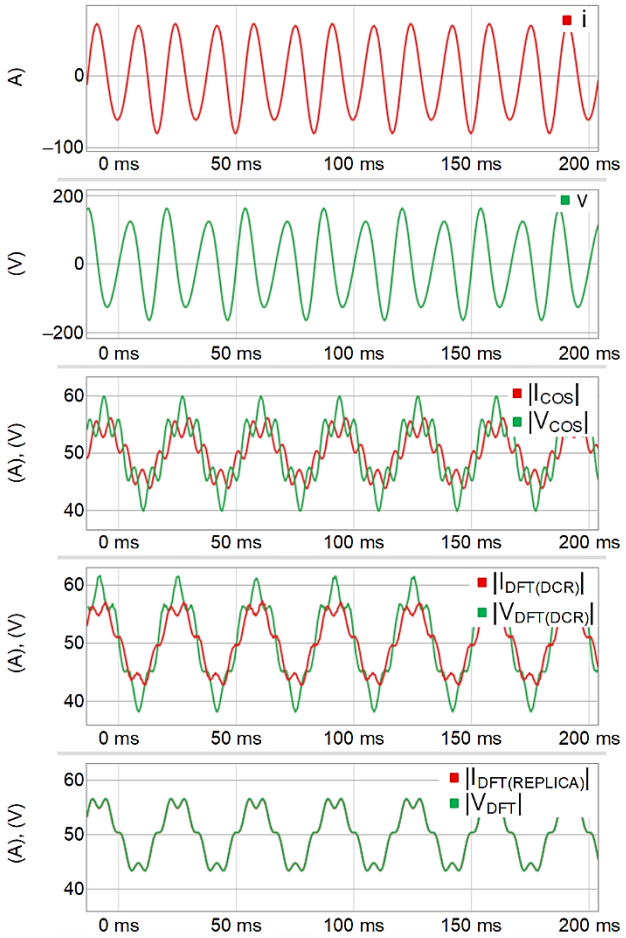


Fig. 12. Filter response to a 90 Hz signal.

Although the interharmonic component passes through all filtering methods, the $FIR_{DFT(REPLICA)}$ algorithm aligns the voltage and current ripple components. Consequently, the calculated apparent impedance remains stable at its expected

value. In contrast, conventional FIR_{COS} and FIR_{DFT} implementations produce oscillatory apparent impedance measurements that vary above and below the true impedance, as seen in Fig. 13.

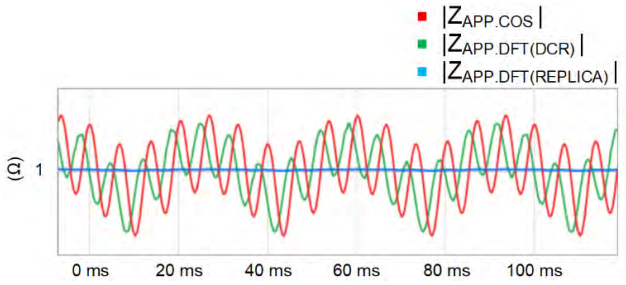


Fig. 13. Apparent impedance calculations of filtering techniques with 90 Hz content in the signal.

The key benefit of the replica current filter is that it aligns all frequency content contained within the measured signals. Apparent impedance calculations therefore remain stable even when interharmonic content is present by letting the voltage and replica current phasor "ripples" to mutually cancel. Without this alignment process, additional frequency content appears directly in the apparent impedance estimate, creating overreach and underreach oscillations. Again, we can see that (6) only holds true if a replica current filter is used.

To further illustrate, we compare $IZ_{COS(REPLICA)}$ to V_{COS} and IZ_{COS} to V_{COS} by converting the phasors to a time-domain representation using (9), as shown in Fig. 14. We can see that there is no difference between $iz_{COS(REPLICA)}$ and v_{COS} ($SOP_{ZAPP.COS[REPLICA]}$), which illustrates the replica current filter properly aligning all frequency content with the voltage. In contrast, the difference between iz_{COS} and v_{COS} ($SOP_{ZAPP.COS}$) contains the 90 Hz content (period of about 11 ms) that was not properly aligned between the two signals.

Although the cosine filter does not require additional filtering for dc removal, it does benefit from the inclusion of a replica current calculation prior to FIR_{COS} to align frequency content not rejected by FIR_{COS}.

Based on this analysis, we can further improve an apparent impedance relay and provide better performance by editing (6) as shown in (11). The FIR used can be either an FIR_{DFT} or FIR_{COS}.

$$|IZ_{FIR(REPLICA)}| \bullet |Z_{APP}| = |V_{FIR}| \tag{11}$$

This shows us that even though an apparent impedance relay operating purely on the nominal frequency signal does not require the maximum torque angle setting ($\angle Z_R$), this information can be used in a replica current filter to provide better performance by providing total rejection of dc content as well as aligning all frequency content not rejected by FIRs.

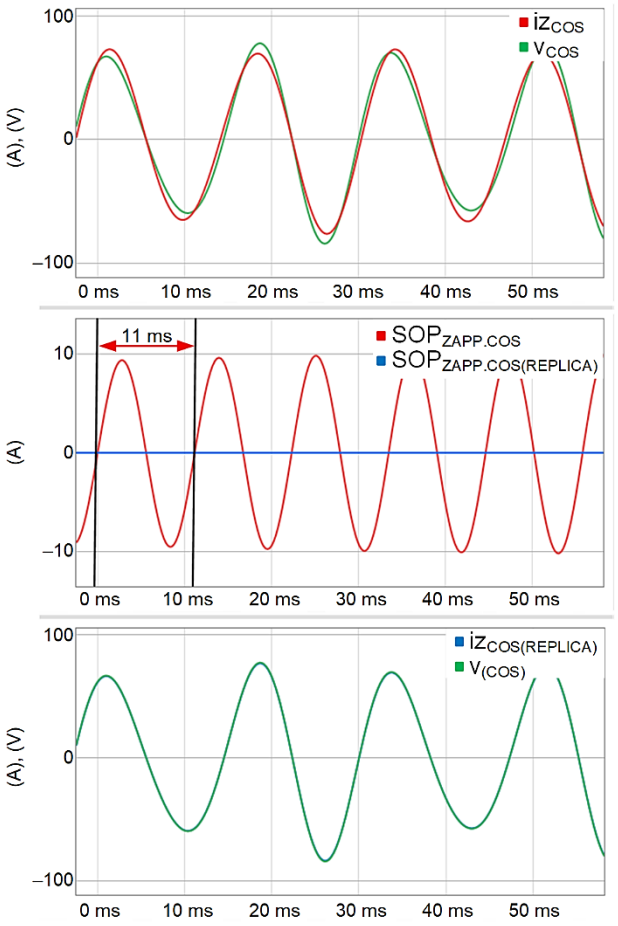


Fig. 14. Comparison of using replica current filter versus not.

IV. Simulation Event

The signals shown in Fig. 15 were obtained from the laboratory model simulation presented in [3] and correspond to a metallic ABG fault. The lower trace illustrates the magnitude of the apparent impedance calculation, $|Z_{APP}|$, for the AB fault loop. Because the availability of measurement time is an important consideration when evaluating apparent impedance performance, the analysis begins with the magnitude of the apparent impedance rather than its trajectory in the apparent impedance plane.

The $|Z_{APP.DFT(REPLICA)}|$ signal represents the apparent impedance calculation obtained using a relay that employs a replica current filter in conjunction with FIR_{DFT}, whereas $|Z_{APP.COS}|$ represents the calculation obtained using FIR_{COS} only. $|Z_{APP.DFT(REPLICA)}|$ is a highly stable and accurate apparent impedance estimate, varying only from 3.16 Ω to 3.21 Ω around the expected value of 3.21 Ω. In contrast, $|Z_{APP.COS}|$ exhibits significant variation, ranging from 2.41 Ω to 4.0 Ω.

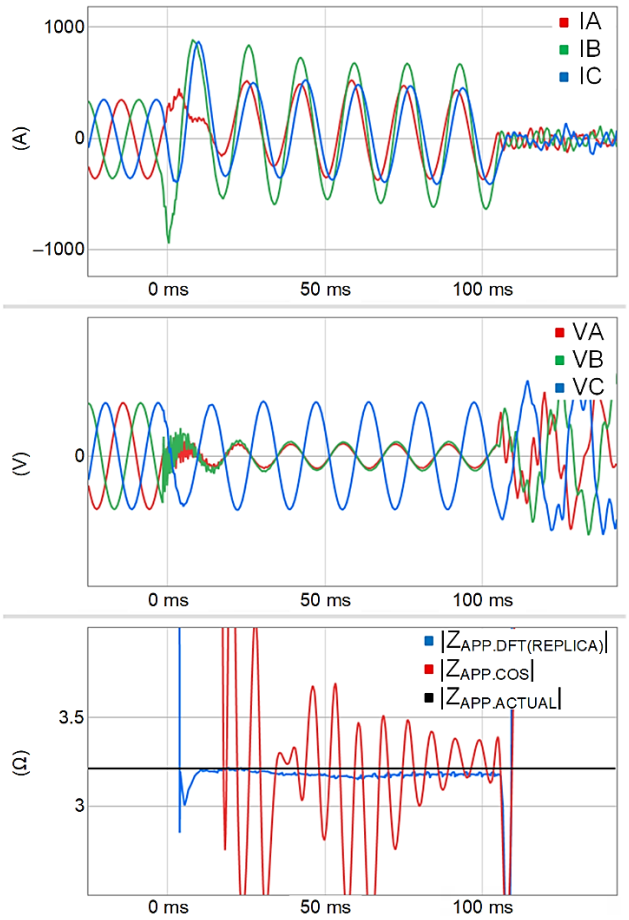


Fig. 15. $|Z_{APP}|$ for an ABG fault from an IBR model simulation.

For reference, the apparent impedance calculations from Fig. 15 are plotted in the apparent impedance plane in Fig. 16. The apparent impedance locus of $Z_{APP.DFT(REPLICA)}$ is sufficiently small enough so that magnification of the highlighted region is required to observe its trajectory. This result demonstrates that the replica current filter preserves both the magnitude and phase-angle relationship between the fault loop voltage and current signals. In contrast, the apparent impedance locus of $Z_{APP.COS}$ exhibits significant movement within the apparent impedance plane. To prevent Zone 1 operations for FIR_{COS} relays near an IBR, [8] recommends a security time delay of 3 cycles. A relay that uses a replica current filter ($FIR_{DFT[REPLICA]}$ or $FIR_{COS[REPLICA]}$) does not require a security time delay.

To better understand the source of the apparent impedance oscillations observed in $Z_{APP.COS}$, Fig. 17 compares the fault loop voltage, the fault loop replica current multiplied by the actual apparent impedance magnitude, and the resulting SOP_{ZAPP} values.

The fault loop replica current is shown using a replica current filter ($iz_{DFT[REPLICA]}$) and not (iz_{COS}). The replica current filter provides an SOP_{ZAPP} signal that is essentially 0 V. However, the SOP_{ZAPP} signal from the relay that does not have replica current filter shows a significant signal oscillation that represents an error after the filtering process. The frequency analysis of this signal shows that there is a 75 Hz oscillation that is not attenuated by the FIR filtering. The replica current filter can align this frequency content so that a stable and accurate apparent impedance calculation is performed.

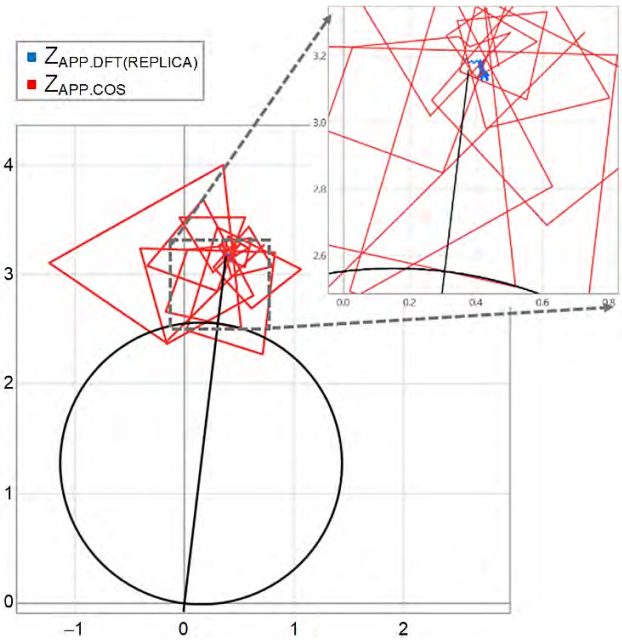


Fig. 16. Apparent impedance calculations for the fault in Fig. 15.

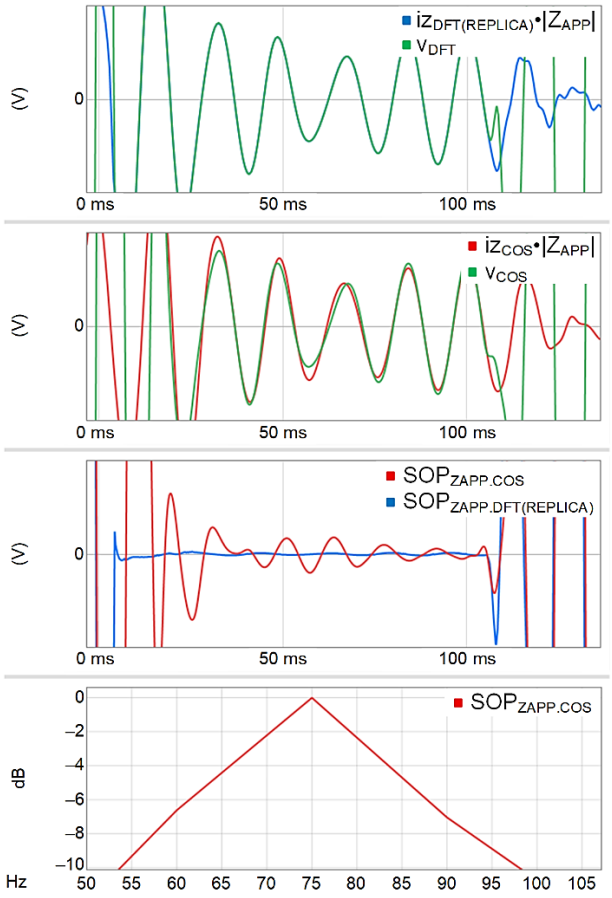


Fig. 17. VAB, IABZ, and ZAB magnitudes from simulation event.

This event illustrates the importance of maintaining time alignment between the fault loop voltage and current signals when interharmonic content is present.

V. Field Event

On June 28, 2025, a Phase C arrester failed on the bus at Substation A resulting in a CG fault, represented in Fig. 18. The bus protection at Substation A successfully detected the fault; however, the FIR_{COS} line relaying at Substation B subsequently overreached and tripped via the Zone 1 ground distance element (ZG1), as observed in Fig. 19. The sources behind the Substation B relay were purely wind generation totaling 600 MW with a mix of Type 3 and Type 4 wind. The Substation B relay voltage connections were fed from capacitive voltage transformers (CVTs).

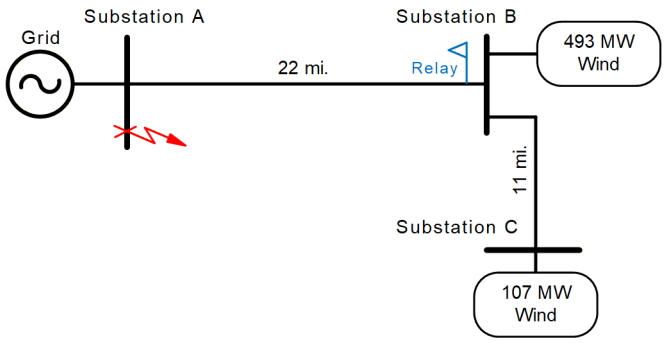


Fig. 18. Transmission system from field event.

The apparent impedance measurements associated with this event are shown in Fig. 19. Analysis of the FIR_{COS} apparent impedance calculation reveals substantial oscillations in the measured apparent impedance, ultimately causing the ZG1 element to overreach and operate for an external fault. To evaluate the performance of replica current filtering, the event was replayed into a relay employing the $FIR_{DFT(REPLICA)}$ algorithm. Like the simulation results presented previously, the $Z_{APP.DFT(REPLICA)}$ apparent impedance calculation remained highly stable, varying only between 2.87 Ω and 2.95 Ω. Consequently, the corresponding ZG1 element remained secure and did not issue a trip.

To better understand the source of the apparent impedance oscillations observed in $Z_{APP.COS}$, Fig. 20 compares the fault loop voltage, the fault loop replica current multiplied by the actual apparent impedance magnitude, and the resulting SOP_{ZAPP} values. The fault loop replica current is shown using a replica current filter ($iz_{DFT[REPLICA]}$) and not (iz_{COS}). The replica current filter provides an SOP_{ZAPP} signal that is essentially 0 V. However, the SOP_{ZAPP} signal from the relay that does not have replica current filter shows a significant signal oscillation that represents an error after the filtering process. The frequency analysis of this signal shows that there is a 90 Hz oscillation that is not attenuated by the FIR filtering. The replica current filter can align this frequency content so that a stable and accurate apparent impedance calculation is performed.

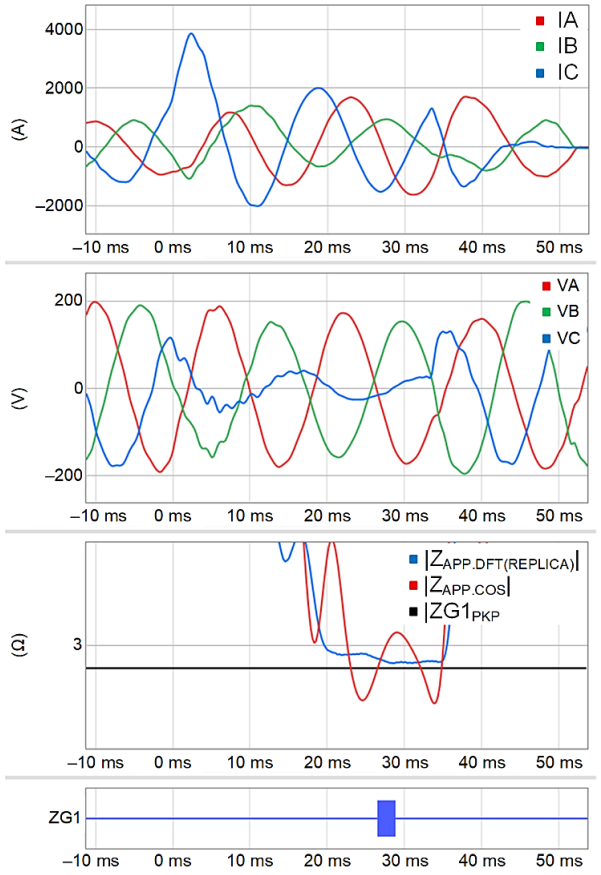


Fig. 19. Field event from IBR with *m* using fault loop polarization.

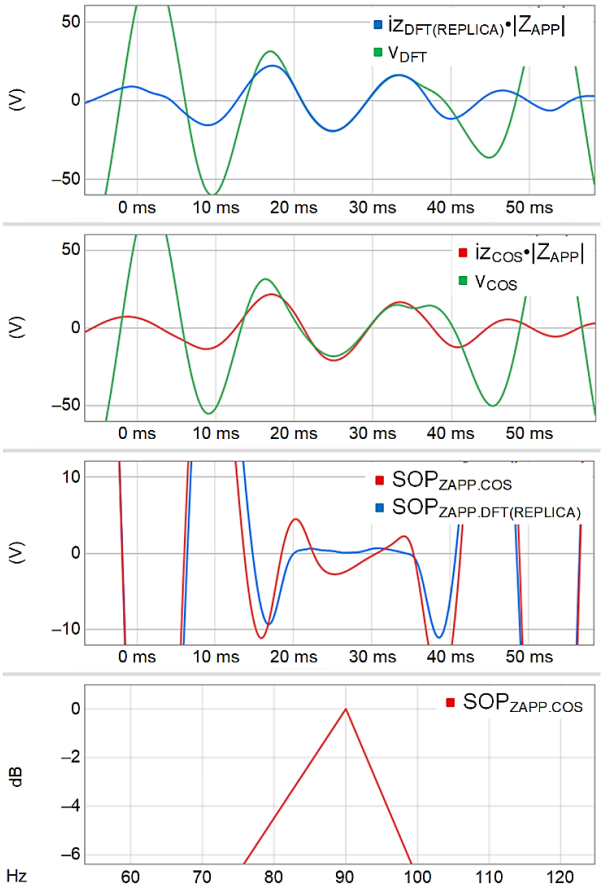


Fig. 20. Field event from IBR with *m* using fault loop polarization.

Although CVTs were used during this event, the frequency response of the voltage measurement was sufficiently accurate to preserve consistency with the frequency content derived from the current signal through the replica current filter. Consequently, the $FIR_{DFT(REPLICA)}$ method maintained alignment between the voltage and current quantities despite the presence of non-fundamental frequency content.

This event provides field validation of the simulation results presented earlier. While both relay implementations were exposed to the same interharmonic rich fault signals, the relay employing the replica current filter maintained a stable apparent impedance measurement and avoided an undesired Zone 1 operation. These results demonstrate the practical benefits of the replica current filter for improving both security and dependability in IBR-dominated power systems.

VI. Conclusions

This paper demonstrates that apparent impedance oscillations in IBR-dominated systems are fundamentally caused by misalignment of off-nominal voltage and current frequency components that survive relay filtering. FIR-based techniques that do not use a replica current filter maintain voltage and current alignment at nominal system frequency, whereas a replica current filter maintains voltage and current alignment across the broader frequency spectrum observed during IBR-fed faults.

While narrowing the FIR bandwidth can improve rejection of these frequencies, it also increases operating time. Replica current filtering provides a more effective solution by mitigating the impact of unrejected frequency components without sacrificing relay speed.

To compensate for oscillatory apparent impedance measurements associated with IBR-fed faults, many conventional FIR_{COS}- and FIR_{DFT}-based relays require distance element security or dependability timers [8]. This practice increases setting complexity and may reduce user confidence in relay performance. Furthermore, the use of self-polarized, nondirectional distance elements proposed for IBR applications does not inherently eliminate impedance oscillations. Without a replica current filter, oscillatory apparent impedance behavior may still be present despite the removal of memory voltage effects.

Replica current filtering leverages the fundamental relationship between voltage and current on the protected transmission line to improve the stability and accuracy of apparent impedance calculations in electrically noisy environments. Consequently, distance protection can be implemented without user-applied security or dependability timers while preserving the performance advantages of self-polarized distance elements.

Additional improvements in apparent impedance accuracy are possible when using wide-spectrum time-domain impedance measurement techniques [5]. Unlike conventional approaches, these methods estimate apparent resistance and inductance directly from the instantaneous loop voltage and current; and therefore, do not require FIR-based phasor extraction. This approach provides a promising path for further improving apparent impedance measurement accuracy in systems containing both fault resistance and significant interharmonic content.

VII. Appendix

Derivation for apparent impedance element that uses a mho characteristic with the offset ZR(OFF) = 0.

$$
\begin{aligned}
&RE(S_{OP} \bullet S_{POL}{}^{*}) > 0 \\
&S_{OP} = I \bullet Z_R - V \\
&S_{POL} = I \bullet Z_{R(off)} + V \\
&Z_{R(OFF)} = 0 \\
&RE((I \bullet Z_R - V) \bullet (V)^{*}) > 0 \\
&RE((I \bullet Z_R \bullet (V)^{*} - V \bullet V^{*}) > 0 \\
&|Z_R| > \frac{|V^2|}{RE[V^{*} \bullet I \bullet 1\angle Z1_{ANG}]} > 0
\end{aligned}
\tag{12}
$$

Derivation for apparent impedance that uses an ohm characteristic using geometry evaluation, which assumes the center is located at the origin in the apparent impedance plane.

$$
\begin{aligned}
&Center = \left[\frac{Z_{R(RE)} + Z_{R(OFF)(RE)}}{2}, \frac{Z_{R(IM)} + Z_{R(OFF)(IM)}}{2} \right] \\
&Radius = \sqrt{\left(Z_{R(RE)} - Center_{(RE)}\right)^2 + \left(Z_{R(IM)} - Center_{(IM)}\right)^2} \\
&|Z_{APP} - Center| < |Z_R - Center| \\
&Center = 0 \\
&|Z_{APP}| < |Z_R| \\
&\frac{|V|}{|I|} < |Z_R|
\end{aligned}
\tag{13}
$$

VIII. References

[1] *SEL-121 Distance Relay Fault Locator Instruction Manual*. Available: selinc.com.

[2] G. Benmouyal, "Removal of DC-Offset in Current Waveforms Using Digital Mimic Filtering," in IEEE Transactions on Power Delivery, vol. 10, no. 2, pp. 621-630, April 1995, doi: 10.1109/61.400869.

[3] R. Chowdhury and N. Fischer, "Transmission Line Protection for Systems With Inverter-Based Resources – Part I: Problems," in IEEE Transactions on Power Delivery, vol. 36, no. 4, pp. 2416-2425, Aug. 2021, doi: 10.1109/TPWRD.2020.3019990.

[4] B. Kasztenny, "Distance Elements for Line Protection Applications Near Unconventional Sources," proceedings of the 75th Annual Conference for Protective Relay Engineers, March 2022.

[5] B. Kasztenny and G. Smelich, "Wideband Distance Protection and Single-Ended Fault-locating Method," proceedings of the 53rd Annual Western Protective Relay Conference, Spokane, WA, October 2026.

[6] D. D. Fentie, "Understanding the Dynamic Mho Distance Characteristic," 69th Annual Conference for Protective Relay Engineers (CPRE), College Station, TX, USA, 2016, pp. 1-15, doi: 10.1109/CPRE.2016.7914922.

[7] E. O. Schweitzer and B. Kasztenny, “Distance protection: Why Have We Started With a Circle, Does it Matter, and What Else is Out There?,” 71st Annual Conference for Protective Relay Engineers (CPRE), College Station, TX, USA, 2018, pp. 1-19, doi: 10.1109/CPRE.2018.8349791.

[8] R. McDaniel, R. Chowdhury, K. Zimmerman, and B. Cockerham, “Applying SEL Relays in Systems With Inverter-Based Resources,” SEL Application Guide (AG2021-37), 2025. Available: selinc.com.

IX. Biographies

Michael Rader Michael attended Michigan Technological University in Houghton, MI, and obtained his BSE in Electrical and Computer Engineering in 2017. After school, he worked for two years as an industrial application engineer, developing testing automation solutions for auto industry clients around Detroit. In 2021, he made the switch to the utility industry. He now works as a Relay Engineer with Minnesota Power and is studying for his PE exam. When not at work, Michael can be found jogging with his dogs or coaching youth soccer in Duluth, MN.

Ryan McDaniel earned his BS in computer engineering from Ohio Northern University in 2002. In 1999, he was hired by American Electric Power (AEP) as a relay technician and a protection and control engineer. In 2005, he joined Schweitzer Engineering Laboratories, Inc. (SEL) and is currently a principal engineer. His responsibilities include providing application support and technical training for protective relay users. Ryan is a registered professional engineer in the state of Illinois and a member of IEEE.

Josh LaBlanc received his BS in electrical engineering from the University of North Dakota in 2011. After graduation, Josh worked for an oil and gas pipeline company, Enbridge Energy, then an electric power utility, Minnesota Power. Josh has most recently spent 6.5 years working as an application engineer for Schweitzer Engineering Laboratories, Inc. (SEL). His primary roles are providing application and technical support and training on power system protection topics. Josh is a registered professional engineer in the state of Minnesota.

Kale McCarthy received his Bachelor of Science degree in electrical engineering with highest honors from Montana Technological University in 2023. He joined Schweitzer Engineering Laboratories, Inc. (SEL) as an intern in 2022 and was then hired as a product engineer in 2023 in the transmission department. In addition to working at SEL, Kale joined Montana Tech in 2025 as an adjunct professor, where he teaches courses in power system protection. He is an active IEEE member.

Bishal Lamichhane earned his BE Electrical Engineering degree in 2014 from Tribhuvan University, Nepal. He worked as an electrical design consultant for three years after school and as an electrical engineer for Nepal Electricity Authority until 2022. He received his MS in Electrical and Computer Engineering in 2024 and worked as a power systems engineer for 1.5 years after graduation. He joined SEL in March 2026 as an application engineer and works on application support and technical training on power systems protection. He is an active IEEE member.

© 2026 by Minnesota Power and
Schweitzer Engineering Laboratories, Inc.
All rights reserved.
20260915 • TP7266-01